MedCrave
Step into the World of Research
Aeronautics and Aerospace Open access Journal

Review Article

Open Access

CrossMark

Robust nonlinear spatial trajectory control of F/A-18 model

Abstract

This article proposes a novel hybrid two-layer control architecture for 3-D spatial trajectory *(x, y, z)* tracking of a F/A-18 aircraft model under parametric uncertainties. First, an outer loop control subsystem is designed based on sliding mode control (SMC) theory. This SMC subsystem accomplishes spatial trajectory *(x, y, z)* and sideslip angle β control using angular velocity vector—comprising roll rate p, pitch rate q, and yaw rate r - as virtual control input, in conjunction with the derivative of the thrust T_x. Second, a composite inner loop control subsystem, including (i) a geometric homogeneity-based finite-time control law and (ii) a super-twisting (STW) control law, is developed. The inner loop control subsystem is designed to control aircraft roll, pitch, and yaw angular velocities (p, q, r) using aileron, elevator, and rudder control surfaces. The inner loop control subsystem achieves finite-time convergence of the actual (p, q, r) to the computed virtual angular rates derived for the outer loop control. Lyapunov analysis establishes the closed-loop system's stability. Simulation results for a 180^0 climbing turn and helical path-following exhibit precise trajectory tracking performance against large parametric uncertainties.

Keywords: hybrid two-layer flight control, F/A-18 aircraft, super-twisting (STW) control, robust finite-time control, 3-D spatial trajectory control, uncertain nonlinear systems

Volume 10 Issue 3 - 2026

Keum W Lee,[1] Kaushik Raj,[2] Sahjendra N Singh[3]

[1]Professor Emeritus, Department of Electronic Engineering, Catholic Kwandong University, Gangwon 25601, Republic of Korea

[2]Research Engineer III, Rheem R&D Lab, 2600 Gunter Park Dr E, Montgomery, USA

[3]Professor, Department of Electrical and Computer Engineering, University of Nevada Las Vegas, Las Vegas, USA

Correspondence: Sahjendra N Singh, Professor, Department of Electrical and Computer Engineering, University of Nevada Las Vegas, Las Vegas, USA

Received: August 12, 2026 | **Published:** August 24, 2026

Introduction

Spatial trajectory control of aircraft is an important area of research. Feedback linearization[1] and input-output map inversion[2] of nonlinear dynamical systems have played key role in developing flight control systems.[1,3–7] But these two design techniques require precise knowledge of model parameters. Researchers have developed robust dynamic inversion methods for flight control.[8–10] For nonlinear uncertain systems, sliding mode control (SMC) systems were proposed.[11,12] Several researchers have designed SMC systems for maneuvering aircraft.[13–15] The SMC laws include switching functions (relays) for suppressing the effect of unknown disturbance inputs and uncertain parameters. But the discontinuity in the control input can cause undesirable control chattering. Subsequently, super-twisting (STW) control systems were developed.[12] The STW control laws are continuous unlike the SMC laws. STW control systems have been designed for rapid large roll-coupled maneuvers of a swept wing fighter aircraft.[16–18] In these articles, two sets of output variables (i) (roll angle ϕ , angle of attack α , sideslip angle β) and (ii) (ϕ , pitch angle θ , β) have been selected for the independent control of outputs by using aileron, elevator, and rudder.

Adaptive control systems are widely used for the control of models including unknown constant parameters.[19–20] Several authors have developed adaptive control laws for the flight control.[21–32] These adaptive systems use parameter estimators to obtain the estimates of the unknown parameters for control law synthesis. Of course, convergence of parameter error is not essential for trajectory tracking. Also, a L_1 adaptive control law has been proposed.[33] In a recent paper,[34] a novel composite adaptive flight control system has been designed for roll-coupled meneuvers of aircraft. Interestingly, the closed-loop system of ([34]) has achieved trajectory regulation and aircraft parameter estimation.

Research has been also done for the spatial trajectory control of different models of aircraft.[35–38] A singular perturbation-based nonlinear control law for 3-D spatial trajectory tracking has been developed.[35] Essentially this design method exploits the two time-scale property of the slow outer loop and fast inner loop. The trajectory control of a VTOL transition aircraft and a generic hypersonic vehicle has been presented in Refs.[37–38] However, in these articles for spatial trajectory control, it has been assumed that the dynamical models are perfectly known. Here interest is in the spatial trajectory control of F/A-18 nonlinear model, which is imprecisely known. Earlier based on SMC and adaptive control techniques, control systems for the 3-D spatial trajectory control have been designed for F/A-18 model.[39,40] For simplicity in design, the complete closed-loop control system was split into an outer loop controller and an inner loop controller. The outer loop controllers of ([39, 40]) are based on SMC technique, but the inner loops have distinct adaptive control laws. The computational burden of adaptive systems increases with the number of unknown model parameters. Certainly, it is desirable to explore the applicability of other robust design methods.

In this paper, robust 3-D spatial trajectory control of the F/A-18 model considered in Refs.[39,40] is considered. The contribution of this paper is two-fold. First, similar to Refs.,[39,40] a sliding mode control law is designed for the spatial trajectory *(x, y, z)* and sideslip angle β control using angular velocity vector (roll rate p, pitch rate q, and yaw rate r) treated as virtual control input $\left(\omega_v \in R^3\right)$ and the derivative of the forward thrust T_x. The choice of β as the fourth component of the controlled output vector is to keep it small during maneuver for limiting any adverse effect of the aerodynamic load. Second, an inner loop control system is formed by (i) a geometric homogeneity-based finite-time control law designed for a nominal model F/A-18 without uncertainty and (ii) a super-twisting (STW) control law for robustification in the presence of model parameter uncertainty. It is should be noted that the homogeneity-based control law and STW law for the inner loop control are continuous functions of time. The inner loop composite control system controls the actual aircraft roll, pitch, and yaw angular velocity vector $\omega = \left(p, q, r\right)^T$ of the aircraft using aileron, elevator, and rudder control surfaces. The goal is to achieve convergence of the error $\left(\omega - \omega_v\right)$ to zero in a finite time. Therefore,

©2026 Lee et al. This is an open access article distributed under the terms of the Creative Commons Attribution License, which permits unrestricted use, distribution, and build upon your work non-commercially.

Copyright: ©2026 Lee et al.

the combined control system (formed by the outer loop SMC law and the finite-time inner loop control law) accomplishes asymptotic 3-D spatial reference trajectory tracking. By the Lyapunov analysis, stability of the closed-loop system is examined. Simulation results for 180^0 climbing turn and helical path following are presented, which confirm accurate trajectory tracking performance in spite of large parametric uncertainties.

Aircraft model and control problem

Often equations of motion of aircraft are represented in different sets of coordinates. The coordinate systems of interest are: an inertial ground axes system (S_g) fixed on (nonrotating) Earth; the local horizontal system (S_h), a translation of S_g, body fixed coordinate frame (S_b) fixed at the center of gravity of the aircraft; the wind axes system (S_w) (obtained by three successive rotations of heading angle (χ), flight path angle (γ), and velocity roll angle (μ)); and the body fixed coordinate system S_b obtained from S_w by rotation (- β) (β is the sideslip angle) and then a rotation α (angle of attack). Of course, S_b is also obtained from S_h by three successive rotations of yaw angle, pitch angle θ , and roll angle ϕ . (Readers may refer to Refs.[41,42] for the rotation matrices relating the coordinate frames.)

We consider here the force equations in S_w and moment equations in S_b. For a complete derivation, readers may refer to. ([41,42]) The inertial position coordinate vector of the aircraft is $X_1 = (x, y, z)^T$ (superscript T denotes matrix transposition) and define $X_2 = (V, \chi, \gamma)^T \in R^3$. The force equations are described by

$$\dot{X}_1 = \begin{pmatrix} \dot{x} \\ \dot{y} \\ \dot{z} \end{pmatrix} = \begin{pmatrix} V\cos\chi\cos\gamma \\ V\sin\chi\cos\gamma \\ -V\sin\gamma \end{pmatrix} \doteq f_{x1}(V, \chi, \gamma) \tag{1}$$

$$\dot{X}_2 = \begin{pmatrix} \dot{V} \\ \dot{\chi} \\ \dot{\gamma} \end{pmatrix} = \begin{bmatrix} -g_0 \sin\gamma \\ 0 \\ -g_0 \cos\gamma / V \end{bmatrix}$$

$$+ \begin{bmatrix} (T_x \cos\alpha\cos\beta - D)/m \\ \{T_x(\sin\alpha\sin\mu - \cos\alpha\sin\beta\cos\mu) - Q\cos\mu + L\sin\mu\}/(mV\cos\gamma) \\ \{T_x(\cos\alpha\sin\beta\sin\mu + \sin\alpha\cos\mu) + Q\sin\mu + L\cos\mu\}/(mV) \end{bmatrix}$$

$$\doteq f_0(V, \gamma) + f_1(T_x, V, \alpha, \beta, \mu) \tag{2}$$

where $\doteq$ denotes equality by definition; m is the mass; g_0 is the gravitational acceleration; V is the velocity of aircraft; T_x is the thrust aligned with the x -axis of S_b; and L, D and Q are the lift, drag, and side forces, respectively, expressed in S_w, given by

$$L = (1/2)\rho V^2 S_r \left(C_{L_0} + C_{L\alpha}\Delta\alpha + C_{L_V}\Delta V + C_{L_{\delta e}}\delta_e \right)$$

$$D = (1/2)\rho V^2 S_r \left(C_{D_0} + C_{D\alpha}\Delta\alpha + C_{D_V}\Delta V \right)$$

$$Q = (1/2)\rho V^2 S_r \left(C_{Q_0} + C_{Q\beta}\beta + C_{Q_V}\Delta V + C_{Q_{\delta r}}\delta_r \right) \tag{3}$$

where $\Delta\alpha$ and ΔV are the perturbations from the trim values, and S_r is the reference area. The set of equations which describe $X_3 = (\mu, \alpha, \beta)^T$, and the angular velocity $\omega = (p, q, r)^T$ in S_b are

$$\dot{X}_3 = \begin{bmatrix} \dot{\mu} \\ \dot{\alpha} \\ \dot{\beta} \end{bmatrix} = \begin{bmatrix} 0 & \sin\gamma + \cos\gamma\sin\mu\tan\beta & \cos\mu\tan\beta \\ 0 & -\cos\gamma\sin\mu\sec\beta & -\cos\mu\sec\beta \\ 0 & \cos\gamma\cos\mu & -\sin\mu \end{bmatrix} (f_0 + f_1)$$

$$+ \begin{bmatrix} \cos\alpha\sec\beta & \sin\alpha\sec\beta & 0 \\ -\cos\alpha\tan\beta & -\sin\alpha\tan\beta & 1 \\ \sin\alpha & -\cos\alpha & 0 \end{bmatrix} \begin{bmatrix} p \\ q \\ r \end{bmatrix} \doteq f_2(T_x, X_2, X_3) + B_{X3}(\alpha, \beta)\omega$$

(4)

$$\begin{bmatrix} \dot{p} \\ \dot{q} \\ \dot{r} \end{bmatrix} = (V/V_0)^2 \begin{bmatrix} l_\beta\beta + l_q q + l_r r + (l_{\beta\alpha}\beta + l_{r\alpha})\Delta\alpha + l_p p \\ m_\alpha\Delta\alpha + m_q q - m_{\dot{\alpha}} p\beta + m_V\Delta V + m_{\dot{\alpha}}(g_0/V)(\cos\theta\cos\phi - \cos\theta_0) \\ n_\beta\beta + n_r r + n_p p + n_{p\alpha} p\Delta\alpha + n_q q \end{bmatrix}$$

$$+ \begin{bmatrix} -i_1 qr \\ i_2 pr \\ -i_3 pq \end{bmatrix} + (V/V_0)^2 \begin{bmatrix} l_{\delta a} & l_{\delta r} & 0 \\ 0 & 0 & m_{\delta e} \\ n_{\delta a} & n_{\delta r} & 0 \end{bmatrix} \delta \doteq f_\omega(X_2, X_3, \omega) + B_\omega\delta$$

(5)

where $\delta = (\delta_a, \delta_r, \delta_e)^T$ is the vector of control surface deflections; V_0 is the velocity at trim; and $l_a = (1/2)\rho V_0^2 S_r b(\partial C_l/\partial a)/I_x$ and $m_a = (1/2)\rho V_0^2 S_r \bar{c}(\partial C_m/\partial a)/I_y$ $(a = \{\alpha, \beta, q, ...\})$ denote the aerodynamic derivatives computed at the trim condition. B and $\bar{c}$ are the reference lateral and longitudinal lengths, respectively; I_x, I_y, and I_z are the principal moments of inertia; and $i_1 = (I_z - I_y)/I_x$, $i_2 = (I_z - I_x)/I_y$, and $i_3 = (I_y - I_x)/I_z$. The factor $(V/V_0)^2$ in the rotational motion has been introduced because these parameters are proportional to the square of velocity. The parameters n_β, $l_{\&}$, etc., are similarly computed at the trim condition. It is assumed that the values of aerodynamic derivatives are not known.

The twelve first-order differential equations given in equations (1) - (4) describe the motion of the aircraft, and $X = (X_1^T, X_2^T, X_3^T, \omega^T)^T = (x, y, z, V, \chi, \gamma, \mu, \alpha, \beta, p, q, r)^T \in R^{12}$ is the minimal set of state variables. In fact, θ and ϕ are functions of the components of X. Of course, the pitch and roll angles also satisfy

$$\dot{\theta} = q\cos\phi - r\sin\phi; \dot{\phi} = p + (q\sin\phi + r\cos\phi)\tan\theta \tag{6}$$

Associated with the system (4), consider the controlled output vector

$$w_c = (x, y, z, \beta)^T \in R^4 \tag{7}$$

Here β is included in w_c, because it is desired to keep the sideslip small during maneuver. Suppose that a smooth reference trajectory $w_r = (x_r, y_r, z_r, \beta_r = 0)^T = (X_{1r}^T, 0)^T \in R^4$ is given. We are interested in deriving a control law so that the controlled output $w_c \in R^4$

Citation: Lee KW, Raj K, Singh SN. Robust nonlinear spatial trajectory control of F/A-18 model. *Aeron Aero Open Access J.* 2026;10(3):145–153. DOI: 10.15406/aaoaj.2026.10.00262

Copyright: ©2026 Lee et al.

asymptotically tracks prescribed reference trajectory $w_r \in R^4$ in spite of uncertainties in the aircraft model. For simplicity the design will be done in two steps. First, an outer loop control system will be designed for the control of W_c. Then an inner loop control law will be derived to achieve convergence of the actual angular velocity w to w_v. The combined control law will accomplish spatial trajectory control.

Sliding mode outer loop control system

Now an outer-loop control system is designed for the trajectory control of $w_c(t)$ using inversion algorithm.[2] This requires successive differentiation of the controlled output vector $w_c(t)$ till the angular velocity $\omega \in R^3$ (treated as virtual control input) and actual input T_x appear. It is seen that X_1 is a function of T_x, but it does not involve the angular velocity vector $\omega \in R^3$. In the third derivative of X_1, w as well as T_x appear. Therefore, now the forward thrust T_x is treated as a state variable, and trajectory control of the output $w_c(t) \in R^4$ by the input $u_p = \left(u_T = \dot{T}_x, \omega^T\right)^T \in R^4$ is considered. Later the inner-loop control system will be designed for the control of actual ω of the aircraft using control surfaces (aileron, elevator, and rudder) so that w converges to the computed virtual w (termed w_v) for the outer-loop control.

Lift, drag, and side forces are functions of the control surface deflections. However, the forces contributed by the control surfaces are small, because these are principally moment producing devices. As such, for the purpose of controller design, these small forces are neglected, but are introduced later in the model for simulation. Then using Eqs. (1) - (5), the differential equation for x_p takes the form

$$\dot{x}_p = f_p\left(x_p\right) + B_p\left(x_p\right)u_p \tag{8}$$

where f_p and B_p are appropriate vector function and matrix, respectively. Let $w_p = (x, y, z)^T$. Define the Lie derivatives of $w_p\left(x_p\right)$ as

$$L_{fp}\, w_p\left(x_p\right) = \left[\frac{\partial w_p\left(x_p\right)}{\partial x_p}\right] f_p\left(x_p\right)$$

$$L_{fp}\, L_{fp}^{j-1} w_p\left(x_p\right) = L_{fp}^{j}\, w_p\left(x_p\right) \tag{9}$$

$$L_{Bp}\, L_{fp}^{j}\, w_p\left(x_p\right) = \left[\frac{\partial L_{fp}^{j}\, w_p\left(x_p\right)}{\partial x_p}\right] B_p\left(x_p\right)$$

Then one can easily show that

$$L_{Bp}\, L_{fp}^{j}\, w_p\left(x_p\right) = 0 \text{ , } for\, j = 0,1 \tag{10}$$

and $L_{Bp}\, L_{fp}^{2}\, w_{c_i}\left(x_p\right) \neq 0$ for $x_p \in \Omega_p \subset R^{10}$, $i = 1,2,3$.

Therefore, it follows that $w_{c_i}, i = 1,2,3$ has relative degree three.

The relative degree of $w_{c_4} = \beta$ is one since w appears in the first derivative of w_{c_4}.

Differentiating w_c gives

$$\begin{pmatrix} \ddot{w}_p \\ \dot{w}_{c_4} \end{pmatrix} = \begin{pmatrix} L_{fp}^{3}\, w_p\left(x_p\right) \\ L_{fp}\, w_{c_4}\left(x_p\right) \end{pmatrix} + \begin{pmatrix} L_{Bp}\, L_{fp}^{2}\, w_p\left(x_p\right) \\ L_{Bp}\, w_{c_4}\left(x_p\right) \end{pmatrix} u_p \tag{11}$$

For a robust control design using the VSC theory, one first selects an appropriate sliding surface on which the trajectory has desirable property. We choose here the sliding surface $s_1 = 0$, where

$$s_1 = \begin{bmatrix} \dddot{\tilde{w}}_p + k_{v2}\ddot{\tilde{w}}_p + k_{v1}\dot{\tilde{w}}_p + k_{v0}\int_0^t \tilde{w}_p\, d\tau \\ \beta + k_{b0}\int_0^t \beta d\tau \end{bmatrix} \tag{12}$$

where $\tilde{w}_p = (x, y, z)^T - \left(x_r, y_r, z_r\right)^T = X_1 - X_{1r}$ is the position error vector, K_{vj} and $k_{b0} > 0$. These gains are chosen so that $s_1 = 0$ yields exponentially stable responses for $\tilde{w}_p$ and β. Integral feedback in Eq. (12) provides additional flexibility for a robust design.

For sliding mode control system design, one differentiates s_1 to obtain

$$\dot{s}_1 = \begin{bmatrix} L_{fp}^{3}\, w_p\left(x_p\right) - \dddot{X}_{1r} + k_{v2}\ddot{\tilde{w}}_p + k_{v1}\dot{\tilde{w}}_p + k_{v0}\tilde{w}_p \\ L_{fp}\beta + k_{b0}\beta \end{bmatrix} + \begin{bmatrix} L_{Bp}\, L_{fp}^{2}\, w_p\left(x_p\right) \\ L_{Bp}\, w_{c4}\left(x_p\right) \end{bmatrix}$$

$$\doteq f_s\left(x_p, t\right) + B_s u_p \tag{13}$$

where t in Eq.(13) denotes the dependence of the functions on X_{1r} and its derivatives. Let $f_s = f_s^* + \Delta f_s$ and $B_s = B_s^* + \Delta B_s$, where f_s^* and B_s^* are the nominal functions and ΔB_p and ΔB_s denote the uncertain portions.

It has been shown in ([39]) that the determinant of the input matrix B_s is nonzero if $\gamma \neq \pm\frac{\pi}{2}$ and

$$\left(T_x \sin\alpha_0 + L\right)\left[T_x + \cos\alpha_0\left(\frac{\partial L}{\partial \alpha}\right) + \sin\alpha_0 \frac{\partial L}{\partial \alpha}\right] \neq 0 \tag{14}$$

For the derivation of control law, invertibility of B_s in the region of interest is essential. It has been found in 39 that in a neighborhood Ω_p of the trim conditions Eq. (14) is satisfied. For trajectory control, maneuver through the region in which singularity lies must be avoided by a proper trajectory planning.

For VSC design, consider a Lyapunov function

$$W_1 = \frac{1}{2} s_1^T s_1 \tag{15}$$

The derivative of W_1 along the solution of Eq. (13) is given by

$$\dot{W}_1 = s_1^T\left[\left(f_s^* + \Delta f_s\right) + \left(B_s^* + \Delta B_s\right)u_p\right] \tag{16}$$

Assumption 1: The uncertain functions satisfy for $X \in \Omega_p$,

$$\| \Delta f_s - \Delta B_s B_s^{*-1} f_s^* \|_\infty \leq \eta_0$$

$$max\left\{\| \Delta B_s B_s^{*-1} \|_2, \| \Delta B_s B_s^{*-1} \|_1\right\} \leq \rho < 1 \tag{17}$$

where $\| \cdot \|_\infty$ denotes the infinity-norm of a vector,

$$\| \Delta B_s B_s^{*-1} \|_2 = \left\{\lambda_{max}\left[\left(\Delta B_s B_s^{*-1}\right)^T\left(\Delta B_s B_s^{*-1}\right)\right]\right\}^{1/2}$$

Citation: Lee KW, Raj K, Singh SN. Robust nonlinear spatial trajectory control of F/A-18 model. *Aeron Aero Open Access J.* 2026;10(3):145–153. DOI: 10.15406/aaoaj.2026.10.00262

Copyright: ©2026 Lee et al.

And $\| \Delta B_s B_s^{*-1} \|_1 = max_j \sum_{i=1}^{4} \left| \left(\Delta B_s B_s^{*-1} \right)_{ij} \right|$ are the induced 2 - and 1-norms of matrix, respectively. Here subscript *ij* denotes the *ij*th element of matrix. The second inequality of Eq. (17) essentially restricts the uncertainty in the matrix B_s.

The design of control law is based on a back stepping design technique. Consider a change of coordinate for the angular velocity vector *w* as

$$\tilde{\omega} = \omega - \omega_v \tag{18}$$

where ω_v is a stabilizing signal, yet to be determined. Then u_p can be expressed as

$$u_p = \left[\dot{T}_x, \omega_v^T \right]^T + \left[0, \tilde{\omega}^T \right]^T = u_c + \left[0, \tilde{\omega}^T \right]^T \tag{19}$$

where $u_c = \left[\dot{T}_x, \omega_v^T \right]^T$.

Substituting Eq. (19) in Eq. (16) yields

$$\dot{W}_1 = s^T [\left(f_s^* + \Delta f_s \right) + \left(B_s^* + \Delta B_s \right) u_c + B_a \tilde{\omega}] \tag{20}$$

where $B_s \left[0, \tilde{\omega}^T \right]^T \equiv B_a \tilde{\omega}$

In view of Eq. (20), one selects a VSC law of the form

$$u_c = B_s^{*-1} \left[-f_s^* - K_2 s_1 - K_1 sgn\left(s_1 \right) \right] \tag{21}$$

where the gain K_1 is a positive real number yet to be determined, $K_2 > 0$ and $sgn\left(s_1 \right) = \left[sgn\left(s_{11} \right), ..., sgn\left(s_{14} \right) \right]^T$ is the sign function.

Substituting Eq. (21) in Eq.(20) gives

$$\dot{W}_1 = s_1^T \left[-K_2 s_1 - K_1 sgn\left(s_1 \right) + \Delta f_s + \Delta B_s B_s^{*-1} \left(-f_s^* - K_2 s_1 - K_1 sgn\left(s_1 \right) \right) + B_a \tilde{\omega} \right]$$

$$\leq -K_2 \| s_1 \|_2^2 - K_1 \| s_1 \|_1 + \| s_1 \|_1 \| \Delta f_s - \Delta B_s B_s^{*-1} f_s^* \|_\infty + \| s_1 \|_2^2 \| B_s B_s^{*-1} \|_2 K_2$$

$$+ \| s_1 \|_1 \| \Delta B_s B_s^{*-1} \|_1 K_1 \| sgn\left(s_1 \right) \|_\infty + s_1^T B_a \tilde{\omega} \tag{22}$$

where Hölder inequality for any two vectors $\xi_i \in R^n$ and $p, q \in [1, \infty]$,

$$\left| \xi_1^T \xi_2 \right| \leq \| \xi_1 \|_p \| \xi_2 \|_q, \frac{1}{p} + \frac{1}{q} = 1 \tag{23}$$

Has been used. Using the bounds given in Assumption 1, one obtains from Eq. (22)

$$\dot{W}_1 \leq -K_2 \left(1 - \rho \right) \| s_1 \|_2^2 - K_1 \left(1 - \rho \right) \| s_1 \|_1 + \| s_1 \|_1 \eta_0 + s_1^T B_a \tilde{\omega} \tag{24}$$

In view of Eq. (24), the gain K_1 is chosen as

$$K_1 \geq \left(1 - \rho \right)^{-1} \left[\eta_0 + \eta^* \right], \eta^* > 0 \tag{25}$$

Using Eq. (25) in Eq. (24) yields

$$\dot{W}_1 \leq -K_2 \left(1 - \rho \right) \| s_1 \|_2^2 - \eta^* \| s_1 \|_1 + s_1^T B_a \tilde{\omega}$$

$$\equiv -K_a \| s_1 \|_2^2 - \eta^* \| s_1 \|_1 + s_1^T B_a \tilde{\omega} \tag{26}$$

According to Eq. (26), for the choice of gain K_1 given in Eq. (25), $\dot{W}_1 < 0$ if $s_1 \neq 0$ and $\tilde{\omega} = 0$. In such a case, s_1 tends to zero which, in view of Eq. (12), implies that $\left(\tilde{w}_p, \beta \right) \to 0$ as $t \to \infty$. However, ω is not a control vector.

Inner loop control system

In the next section, the design of the inner loop control system is considered to force $\tilde{\omega}$ to zero. The inner loop control system includes (i) a control subsystem based on geometric homogeneity and (ii) a super-twisting control subsystem for robustification.

Geometric homogeneity-base inner-loop control subsystem

The rotational motion of aircraft from Eq. (5) is rewritten as

$$\dot{\omega} = \begin{pmatrix} \dot{p} \\ \dot{q} \\ \dot{r} \end{pmatrix} = f_\omega \left(X_2, X_3, \omega \right) + B_\omega \delta \tag{27}$$

where $\delta = \left(\delta_a, \delta_r, \delta_e \right)^T \in R^3$. Here interest is in the design of δ to force $\tilde{\omega}$ to zero. The derivative of $\tilde{\omega}$ satisfies

$$\dot{\tilde{\omega}} = f_\omega \left(X_2, X_3, \omega \right) + B_\omega \delta - \dot{\omega}_v \tag{28}$$

where $\dot{\omega}_v$ can be obtained by differentiating ω_v and substituting various derivatives of the state variables. To this end, $f_w \in R^3$ and $B_w \in R^{3\times3}$ are decomposed as

$$f_w = f_w^* + \Delta f_w ; B_w = B_w^* + \Delta B_w \tag{29}$$

where f_w^* and B_w^* are the nominal values, and Δf_w and ΔB_w are unknown parts. It is assumed that $\| \left(B_w^* \right)^{-1} \Delta B_w \| < 1$. Then, Eq. (28) can be written as

$$\dot{\tilde{\omega}} = \left(f_w^* + \Delta f_w \right) + \left(B_w^* + \Delta B_w \right) \delta - \dot{\omega}_d \equiv f_3^* + \Delta g + B_w^* \delta \tag{30}$$

where $f_3^* = f_w^* - \dot{\omega}_d$ is a known part and $\Delta g = \Delta f_w + \Delta B_w \delta$ is an unknown function. In view of Eq. (30), the control input is chosen as

$$\delta = B_w^{*-1} \left[-f_3^* + u_f + u_r \right] \tag{31}$$

where u_f is a finite-time stabilizing signal for the system with $\Delta g = 0$, and u_r is a signal for robustification. Substituting Eq. (31) in Eq. (30) gives

$$\dot{\tilde{\omega}} = \Delta g + u_f + u_r \tag{32}$$

Define $y = \tilde{w} = \left[\tilde{p}, \tilde{q}, \tilde{r} \right]^T = \left[y_1, y_2, y_3 \right]^T \in R^3$ and $u_f = \left[u_{f1}, u_{f2}, u_{f3} \right]^T$. The homogeneity-based control input u_f is selected as[43]

$$u_{fi} \left(y_i \right) = -l_i sgn\left(y_i \right) \left| y_i \right|^{\mu_i}, i = 1, 2, 3 \tag{33}$$

The feedback gains l_i are chosen such that the polynomial

$$\Pi_3 \left(s \right) = s + l_i \tag{34}$$

is Hurwitz. The exponents μ_i are chosen to satisfy $\mu_i \in \left(0, 1 \right)$. Using

Copyright: ©2026 Lee et al.

Eq. (33) in Eq. (32), the derivative of *y* takes the form:

$$\dot{y} = \dot{\tilde{\omega}} = -\begin{bmatrix} l_1 sgn\left(y_1\right)\left|y_1\right|^{\mu_1} \\ l_2 sgn\left(y_2\right)\left|y_2\right|^{\mu_2} \\ l_3 sgn\left(y_3\right)\left|y_3\right|^{\mu_3} \end{bmatrix} + \left(\Delta g + u_r\right) \tag{35}$$

where $l_i, i = 1,2,3$ are positive constants and $\mu_i \in (0,1), i = 1,2,3$. For $\Delta g = 0$ and $u_r = 0$, the system (35) is finite-time stable; that is, its trajectory *y(t)* converges to the origin y=0 in a finite time.

Super-Twisting (STW) inner loop control subsystem

Now, the design of a robustifying control signal u_r is considered for the system Eq. (35) when $\Delta g \neq 0$. Define the new variables $s_2 \in R^3$ and $\xi \in R^3$, satisfying

$$s_2 = y + \xi \in R^3, \dot{\xi} = -u_f\left(y\right) \tag{36}$$

Then differentiating s_2 gives

$$\dot{s}_2 = \Delta g + u_f + u_r + \dot{\xi} = \Delta g + u_r \tag{37}$$

It is of interest to design u_r such that the trajectory of the system reaches the sliding surface $s_2 = 0$ in a finite time, and subsequently remains confined to it. There exists a variety of control signals that can force the system in the sliding mode. Here, an STW control law is selected of the form:[12,44]

$$u_r = -p_1\left|s_2\right|^{1/2} sign\left(s_2\right) + \eta$$
$$\dot{\eta} = -p_2 sign\left(s_2\right) \tag{38}$$

where p_1 and p_2 are appropriate positive constants. Substituting Eq. (38) in (37) gives

$$\dot{s}_2 = \Delta g - p_1\left|s_2\right|^{1/2} sign\left(s_2\right) + \eta, p_1 = 1.5\sqrt{L_p}$$
$$\dot{\eta} = -p_2 sign\left(s_2\right), p_2 = 1.1L_p \tag{39}$$

Define $\eta_b = \Delta g + \eta$. Then Eq. (39) gives

$$\dot{s}_2 = -p_1\left|s_2\right|^{1/2} sign\left(s_2\right) + \eta_b$$
$$\dot{\eta}_b = -p_2 sign\left(s_2\right) + g_u\left(t\right) \tag{40}$$

where $g_u = d\left(\Delta g\right)/dt$. It is assumed that the trajectories evolve in a region $\Omega \subset R^{12}$ of the state space in which the uncertain function g_u satisfies

$$\left|g_u\right| = \left|\frac{d\Delta g\left(.\right)}{dt}\right| \leq L_p \tag{41}$$

where L_p is a sufficiently large positive constant. The STW control law achieves finite-time convergence of s_2 to zero. Therefore, (37) implies that $\Delta g + u_r$ becomes zero after a finite time. Then (32) simplifies to

$$\dot{\tilde{\omega}} = u_f \tag{42}$$

which is finite-time stable. However, it should be noted that the SMC law designed for the outer loop accomplishes asymptotic convergence of tracking error $\tilde{w}_p$ because the sliding surface $s_1 = 0$ in (12) is linear.

Remark 1: We note that $\dot{\omega}_v$ used in Eq. (28) is a complex function of state variables. As such a practical way to obtain an approximate $\dot{\omega}_v$ is to pass ω_v through a filter of the form

$$H_d\left(s\right) = \frac{s}{\tau s + 1} \tag{43}$$

where $\tau \ll 1$. Then following the similar steps of this section, inner loops can be designed. Of course, higher-order accurate differentiator can be designed following Ref. [12] for synthesis.

Simulation results

This section presents results of simulation for the flight path control of a simplified FA-18 model (see ([39]) for model parameters). The complete closed-loop system including the outer loop SMC law and inner loop robust finite-time control law is simulated. Two flight conditions, (*H=30,000* (ft), *M=0.7*) (FC1) and (*H=25,000* (ft), *M=0.8*) (FC2), are considered for simulation, where *H* is the altitude and *M* is the Mach number. Although, derivation of controller is based on a simplified aircraft model, neglected control forces are introduced in the model for simulation. The aerodynamic parameters of Ref.[39] are used for simulation.

The feedback gains are $\left(k_{v0}, k_{v1}, k_{v2}, k_{b0}\right) = \left(3.375I_3, 6.75I_3, 4.5I_3, 1.5\right)$ in Eq. (12), K_1, K_2=(1.5, 1.5) in Eq. (21), $\left(l_1, l_2, l_3, \mu_1, \mu_2, \mu_3\right)$ = (1, 1.2, 1.3, 6/7,6/7,6/7) in Eq. (35), L_p = *0.2* in Eq. (38), and $\tau = 0.005$ in Eq. (43). For the purpose of illustration, reference trajectory $\left(V_r, \chi_r, \gamma_r\right)$ is generated by third order filters are

$$\left(s + \lambda_v\right)^3 V_r = \lambda_v^3 V^*, \left(s + \lambda_\chi\right)^3 \chi_r = \lambda_\chi^3 \chi^*, \left(s + \lambda_\gamma\right)^3 \gamma_r = \lambda_\gamma^3 \gamma^* \tag{44}$$

where *V**, *X**, and γ^* are the command inputs. The poles of these three filters are at -0.2. The reference inertial position trajectory $X_{1r} = \left(x_r, y_r, z_r\right)$, and its derivatives $\dot{X}_{1r}, \ddot{X}_{1r}, \dddot{X}_{1r}$ are constructed using $\left(V_r, \chi_r, \gamma_r\right)$ and its derivatives generated by the filters, and the kinematic Eq. (1). Two kinds of maneuvers are considered. These are a 180^0 climbing turn and climbing a helical path. For robustness analysis, control system is designed using off-nominal values of the aerodynamic derivatives. For simulation, the sign functions in the stabilizing control laws equations (35) and (39) are replaced by the saturation function (sat(.)), where sat $\left(t\right) = t/\epsilon$ if $\left|t\right| < \epsilon$, and sat (t) = sign (t), if $\left|t\right| < \epsilon$. For simulation ϵ=0.001 has been used. For $\dot{\omega}_v$, Eq. (43) is used where τ is chosen as 0.005.

A1. Closed-loop control at FC1: climbing path and helical path

The complete closed-loop system using sliding mode outer loop and robust finite-time inner loop control systems is simulated. For the outer loop design, nominal values of parameters are assumed to be 70% lower than the actual values. In order to avoid control chattering a continuous approximation of *sgn* function by saturation function is used for simulation.

First simulation is done for FC1. The initial conditions are

Citation: Lee KW, Raj K, Singh SN. Robust nonlinear spatial trajectory control of F/A-18 model. *Aeron Aero Open Access J.* 2026;10(3):145–153.
DOI: 10.15406/aaoaj.2026.10.00262

$(x(0)=y(0)=0, z(0)=-H, V(0)=V=696.39\ [\text{ft/s}], \chi(0)=0, \gamma(0)=0,$

$\alpha(0)=\alpha_0=0.0691[rad], \beta(0)=0, \mu(0)=0, \phi(0)=0, \theta(0)=\alpha_0, \omega(0)=0$

Smooth velocity, heading angle, and flight path angle trajectories are generated by the third-order filters for 180degree turn using the reference input $(V^*, \chi^*, \gamma^*)=(V_0, 0, 0)$ for $t\in[0,10)$ and, $(V+50, 180[\text{deg}], 20[\text{deg}])$ for $t\geq 10$. For helical path control, reference trajectory is generated using heading angle turn rate of 6 [deg/s], $V^*=V_0+50(ft/s), \chi^*=6(t-10)[\text{deg}]$, and $\gamma^*=20[\text{deg}]$ for $t\geq 10[\text{sec}]$. These signals are used to construct the reference position trajectories. The reference sideslip angle is zero. Simulated responses for 180^0 turn are shown in Figure 1 and Figure 2. Those for helical path following are shown in Figure. 3 and Figure 4. In the figures, (E_{rx}, E_{ry}, E_{rz}) denotes the position tracking error $\tilde{w}_p$. We observe smooth trajectory following in these figures.

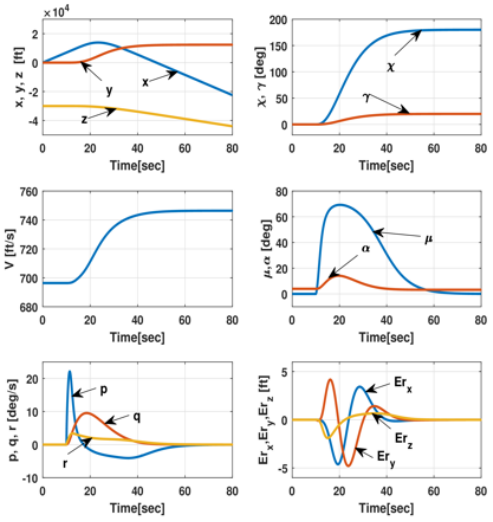

Figure 1 Climbing 180^0 turn at FC1:Top to bottom (left column), (*x, y, z*), *V*, (*p, q, r*), Top to Bottom (right column) (χ,γ), (μ,α), tracking error $(\text{Er}_x, \text{Er}_y, \text{Er}_z)$.

For 180^0 turn, maximum tracking errors $\left(|E_{rx}|, |E_{ry}|, |E_{rz}|\right)_{max}=(4.6127,\ 4.7879,\ 1.8943)[ft]$, steady state tracking errors $\left(|E_{rx}|, |E_{ry}|, |E_{rz}|\right)(t_f)=(0.2316, 0.6025, 0.4294)\times 10^{-3}$ [ft] as shown in Figure 1, maximum trust $T_{x(max)}$ = 19,206[lb], maximum control deflections $(\delta_a, \delta_r, \delta_e)_{max}$ = (3.8127, 1.9190, 6.2162)[deg], and steady state control deflections $(\delta_a, \delta_r, \delta_e)(t_f)$ = (0.0009, 0.0003, 0.0097)[deg] as shown in Figure 2 where t_f = 80 [sec]. For helical path following, maximum tracking errors $\left(|E_{rx}|, |E_{ry}|, |E_{rz}|\right)_{max}$ = (7.1885, 6.7945, 1.6778)[ft], steady state tracking errors $\left(|E_{rx}|, |E_{ry}|, |E_{rz}|\right)(t_f)$ = (5.1728 3.5841 0.0004)[ft] as shown in Figure 3, maximum trust $T_{x(max)}$ = 23,763[lb], maximum control deflections $(\delta_a, \delta_r, \delta_e)_{max}$ = (2.5974, 1.3176, 7.0267)[deg], and steady state control deflections $(\delta_a, \delta_r, \delta_e)(t_f)$ = (0.5081, 0.2265, 6.1839)[deg] as shown in Figure 4. However we observe oscillatory *x* and *y* position tracking error for helical path tracking. This is apparently due to simplified inner loop design in which nominal function have been set to zero.

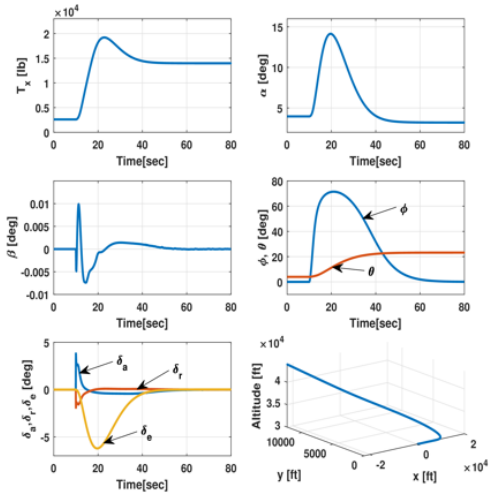

Figure 2 Climbing 180^0 turn at FC1: Top to bottom (left column) $(T_x, \beta, (\delta_a, \delta_r, \delta_e)$, Top to bottom (right column), $(\alpha), (\phi, \theta)$, 3-D plot (*x, y, Altitude*).

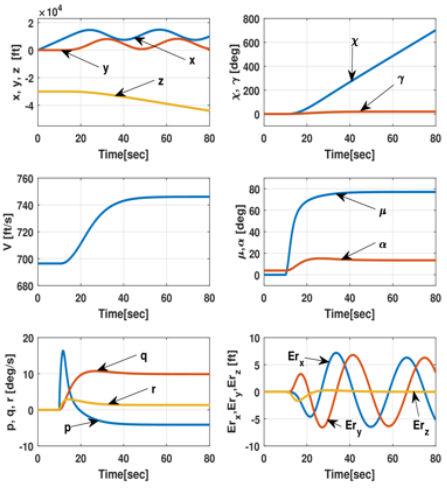

Figure 3 Helical path control at FC1:Top to bottom (left column), (*x, y, z*), *V*, (*p, q, r*), Top to Bottom (right column) (χ,γ), (μ,α), tracking error $(\text{Er}_x, \text{Er}_y, \text{Er}_z)$.

Citation: Lee KW, Raj K, Singh SN. Robust nonlinear spatial trajectory control of F/A-18 model. *Aeron Aero Open Access J.* 2026;10(3):145–153. DOI: 10.15406/aaoaj.2026.10.00262

Copyright: ©2026 Lee et al.

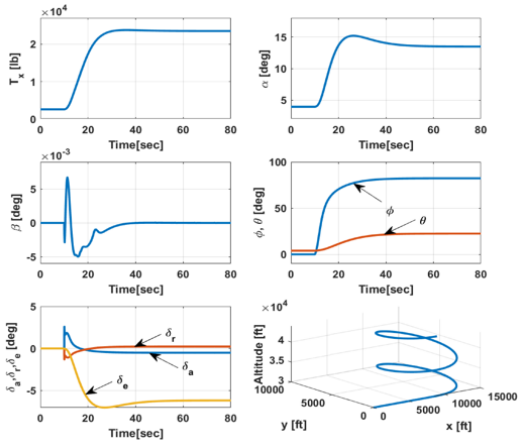

Figure 4 Helical path control at FC1: Top to bottom (left column) $(T_x, \beta, (\delta_a, \delta_r, \delta_e)$, Top to bottom (right column), $(\alpha), (\phi, \theta)$, 3-D plot (*x, y, Altitude*).

A2. Closed-loop control at FC2: climbing path and helical path

Flight condition FC2 is simulated, but the feedback gains of the outer and the inner loops designed for case A1 are retained. Simulated responses for 180^0 turn are shown in Figure 5 and Figure 6. Those for helical path following are shown in Figure 7 and Figure 8. We also observe smooth trajectory following.

For 180^0 turn, maximum tracking errors $\left(|E_{rx}|, |E_{ry}|, |E_{rz}|\right)_{max}$ = (6.9875, 7.2683, 2.52 22)[ft], steady state tracking errors $\left(|E_{rx}|, |E_{ry}|, |E_{rz}|\right)(t_f) = (0.2068, 0.1960, 0.5157) \times 10^{-3}$ [ft] as shown in Figure 5, maximum trust $T_{x(max)}$ = 16,847[lb], maximum control deflections $(\delta_a, \delta_r, \delta_e)_{max}$ = (2.9820, 0.7925, 5.1556)[deg], and steady state control deflections $(\delta_a, \delta_r, \delta_e)(t_f)$ = (0.0189, 0.0020, 0.8759) [deg] as shown in Figure 6 where t_f = 80 [sec]. For helical path following, maximum tracking errors $\left(|E_{rx}|, |E_{ry}|, |E_{rz}|\right)_{max}$ = (11.3897, 10.9421, 2.2733)[ft], steady state tracking errors $\left(|E_{rx}|, |E_{ry}|, |E_{rz}|\right)(t_f)$ = (8.0318, 6.4432, 0.0006)[ft] as shown in Figure 7, maximum trust $T_{x(max)}$ = 20,432[lb], maximum control deflections $(\delta_a, \delta_r, \delta_e)_{max}$ = (2.1193, 0.5700, 6.1582)[deg], and steady state control deflections $(\delta_a, \delta_r, \delta_e)(t_f)$ = (0.4879, 0.0947, 5.7843)[deg] as shown in Figure 8. However we also observe oscillatory *x* and *y* position tracking error for helical path tracking.

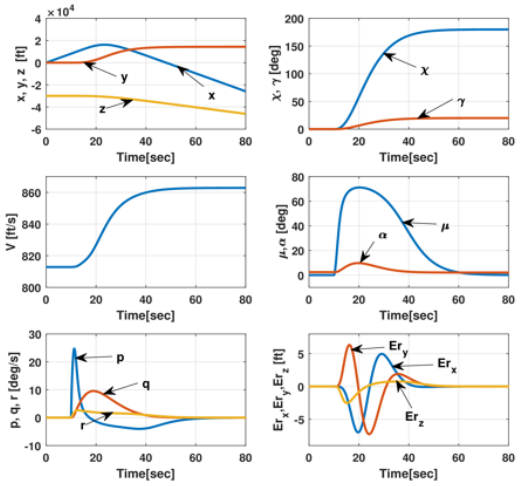

Figure 5 Climbing 180^0 turn at FC1:Top to bottom (left column), (*x, y, z*), *V*, (*p, q, r*), Top to Bottom (right column) (χ, γ), (μ, α), tracking error $\left(\mathrm{Er_x}, \mathrm{Er_y}, \mathrm{Er_z}\right)$.

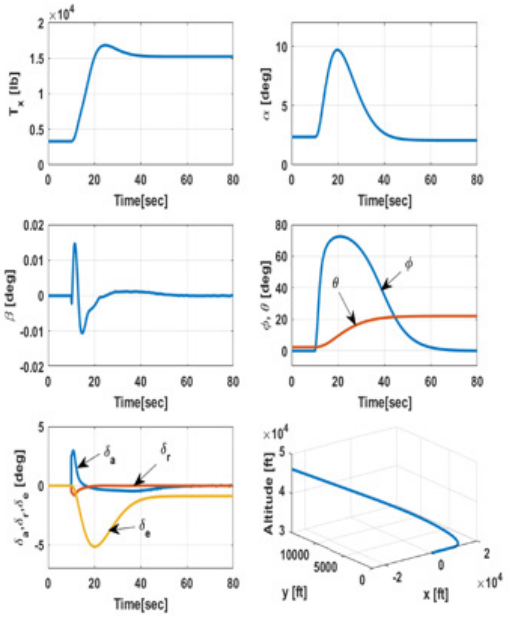

Figure 6 Climbing 180^0 turn at FC1: Top to bottom (left column) $(T_x, \beta, (\delta_a, \delta_r, \delta_e)$, Top to bottom (right column), $(\alpha), (\phi, \theta)$, 3-D plot (*x, y, Altitude*).

Citation: Lee KW, Raj K, Singh SN. Robust nonlinear spatial trajectory control of F/A-18 model. *Aeron Aero Open Access J.* 2026;10(3):145–153. DOI: 10.15406/aaoaj.2026.10.00262

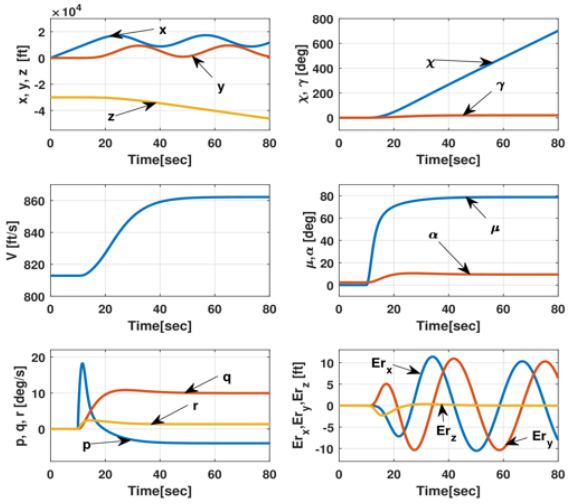

Figure 7 Helical path control at FC2: Top to bottom (left column), (*x, y, z*), *V*, (*p, q, r*), Top to Bottom (right column) (χ,γ), (μ,α), tracking error $\left(\mathrm{Er}_x,\mathrm{Er}_y,\mathrm{Er}_z\right)$.

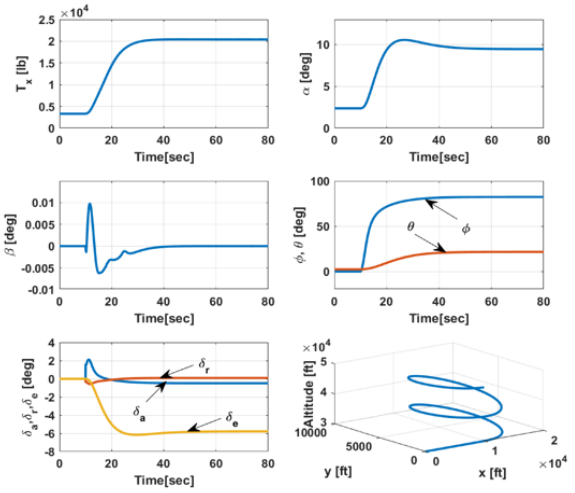

Figure 8 Helical path control at FC2: Top to bottom (left column) $(T_x,\beta,(\delta_a,\delta_r,\delta_e)$, Top to bottom (right column), $(\alpha),(\phi,\theta)$, 3-D plot (*x, y, Altitude*).

Conclusion

This article proposed a composite two-layer architecture for the 3-D spatial trajectory tracking of a nonlinear uncertain F/A-18 aircraft model. First, an outer loop sliding mode control (SMC) system was designed to achieve 3-D spatial trajectory *(x, y, z)* and β control using a virtual angular velocity, termed w_v, and the derivative of forward thrust. Then for the inner loop, (i) a nonlinear nominal control law based on geometric homogeneity and (ii) a super-twisting control law were designed. These two inner loop control laws are continuous. The inner loop control systems achieved finite-time convergence of the roll, pitch, and yaw angular rates (*p, q, r*) to the computed virtual angular velocity w_v. Stability of the closed-loop system was established through Lyapunov analysis. Simulation results for a 180^0 turn and helical path following were obtained. It is observed that the complete closed-loop control system accomplishes precise and smooth 3-D spatial trajectory control in spite of uncertainties in the nonlinear F/A-18 model parameters.

Acknowledgments

None.

Conflict of Interest

The authors declare that there is no conflict of interest.

Funding

None.

References

1. Meyer G, Su R, Hunt LR. Application of nonlinear transformations to automatic flight control. *Automatica*. 1984;20(1):103–107.
2. Singh SN. A modified algorithm for invertibility in nonlinear systems. *IEEE Trans Autom Control*. 1981;26:595–598.
3. Singh SN, Schy AA. Output feedback nonlinear decoupled control synthesis and observer design for maneuvering aircraft. *Int J Control*. 1980;31(4):781–806.
4. Lane SH, Stengel RF. Flight control design using nonlinear inverse dynamics. *Automatica*. 1988;24(4):471–484.
5. Snell SA, Enns DF, Garrad WL. Nonlinear inversion flight control for a supermaneuverable aircraft. *J Guid Control Dyn*. 1992;15(4):976–984.
6. Azam M, Singh SN. Invertibility and trajectory control for nonlinear maneuvers for aircraft. *J Guid Control Dyn*. 1994;17(1):192–200.
7. Bugajski DJ, Enns DF, Elgersma MR. A dynamic inversion based control law with application to a high angle-of-attack research vehicle. In: *Proceedings of the AIAA Guidance, Navigation, and Control Conference*. AIAA; 1990:826-839. AIAA Paper 90–3407.
8. Enns D. Robustness of dynamic inversion vs μ-synthesis: lateral directional flight control example. In: *Proceedings of the AIAA Guidance, Navigation, and Control Conference*. AIAA; 1990:210-222. AIAA Paper 90–3338.
9. Reiner J, Balas GJ, Garrad WL. Robust dynamic inversion for control of highly maneuverable aircraft. *J Guid Control Dyn*. 1995;18(1):18–24.
10. Adams RJ, Banda SS. Robust flight control design using dynamic inversion and structured singular value synthesis. *IEEE Trans Control Syst Technol*. 1993;1(2):80–92.
11. Slotine JJE, Li W. *Applied Nonlinear Control*. Prentice-Hall; 1991:276-309.
12. Shtessel Y, Edwards C, Fridman L, et al. *Sliding Mode Control and Observation*. Birkhäuser; 2014.
13. Gopalaswamy S, Hedrick JK. Tracking nonlinear nonminimum phase systems using sliding control. *Int J Control*. 1993;57(5):1141–1158.
14. Shtessel Y, Buffington J, Banda S. Multiple time scale flight control using reconfigurable sliding modes. *J Guid Control Dyn*. 1999;22(6):873–883.
15. Shkolnikov IA, Shtessel YB. Aircraft nonminimum phase control in dynamic sliding manifolds. *J Guid Control Dyn*. 2001;24(3):566–567.
16. Raj K, Muthukumar V, Singh SN, et al. Finite-time sliding mode and super-twisting control of fighter aircraft. *Aerosp Sci Technol*. 2018;82-83:487–498.
17. Raj K. *Fighter Aircraft Guidance and Control*. PhD dissertation. Department of Electrical and Computer Engineering, University of Nevada, Las Vegas; 2020.

Copyright: ©2026 Lee et al.

18. Raj K, Muthukumar V, Singh SN, et al. Robust higher-order sliding mode control systems for roll-coupled maneuvers of aircraft using output feedback. In: *2018 Atmospheric Flight Mechanics Conference*. American Institute of Aeronautics and Astronautics; 2018. AIAA Paper 2019-3180.
19. Narendra KS, Annaswamy AN. *Stable Adaptive Systems*. Prentice-Hall; 1989.
20. Ioannou PA, Sun J. *Robust Adaptive Control*. Prentice-Hall; 1995.
21. Singh SN, Steinberg ML. Adaptive control of feedback linearizable nonlinear systems with application to flight control. *J Guid Control Dyn*. 1996;19(4):871–877.
22. Farrell J, Sharma M, Polycarpou M. Backstepping–based flight control with adaptive function approximation. *J Guid Control Dyn*. 2005;28(6):1089–1102.
23. Farrell JA, Polycarpou MM, et al. Adaptive backstepping with magnitude, rate, and bandwidth constraints: aircraft longitude control. In: *Proceedings of the American Control Conference*. 2003:3898–3903.
24. Sharma M, Ward DG. Flight–path angle control via neuro–adaptive backstepping. In: *AIAA Guidance, Navigation, and Control Conference and Exhibit*. American Institute of Aeronautics and Astronautics; 2002.
25. Calise AJ, Lee S, Sharma M. Development of a reconfigurable flight control law for tailless aircraft. *J Guid Control Dyn*. 2001;24(5):896–902.
26. Suresh S, Omkar SN, Mani V, et al. Nonlinear adaptive neural controller for unstable aircraft. *J Guid Control Dyn*. 2005;28(6):1103–1111.
27. Sonneveldt L, Chu QP, Mulder JA. Nonlinear flight control design using constrained adaptive backstepping. *J Guid Control Dyn*. 2007;30(2):322–336.
28. Shin DH, Kim Y. Reconfigurable flight control system design using adaptive neural networks. *IEEE Trans Control Syst Technol*. 2004;12(1):543–550.
29. Xu H, Mirmirani D, Ioannou PA. Adaptive sliding mode control design for a hypersonic flight vehicle. *J Guid Control Dyn*. 2004;27(5):829–838.
30. Calise AJ, Rysdyk R. Nonlinear adaptive flight control using neural networks. *IEEE Control Syst Mag*. 1998;18(6):14–25.
31. Balakrishnan SN, Biega V. Adaptive–critic–based neural networks for aircraft optimal control. *J Guid Control Dyn*. 1996;19(4):893–898.
32. Lee KW, Nambisan P, Singh SN. Adaptive variable structure control of aircraft with an unknown high–frequency gain matrix. *J Guid Control Dyn*. 2008;31(1):194–203.
33. Wang J, Patel VV, Cao C, et al. Novel L1 adaptive control methodology for aerial refueling with guaranteed transient performance. *J Guid Control Dyn*. 2008;31(1):182–193.
34. Lee KW, Singh SN, Raj K. Composite adaptive roll–coupled aircraft maneuvers and parameter estimation. In: *SciTech 2025 Forum*. American Institute of Aeronautics and Astronautics; 2025. AIAA Paper 2025–2078.
35. Menon PKA, Badgett ME, Walker RA, et al. Nonlinear flight test trajectory controllers for aircraft. *J Guid Control Dyn*. 1987;10(1):67–72.
36. Oznalbant Z, Chakravarthy A, Dogan A. Determination of control inputs of a fixed–wing aircraft for a given spatial trajectory. In: *AIAA SciTech Forum*. 2020; Orlando, FL.
37. Bhardwaj P, Holzapfel F. Unified trajectory control for vertical take–off and landing transition aircraft. In: *AIAA Aviation Forum and Ascend*. 2024; Las Vegas, NV.
38. Hattis P, Malchow H, Shaughnessy J, et al. Integrated trajectory and control analysis for generic hypersonic vehicles. In: *Proceedings of the 3rd International Aerospace Planes Conference*. 1991; Orlando, FL.
39. Singh SN, Steinberg M, Page AB. Nonlinear adaptive and sliding mode flight path control of F/A–18 model. *IEEE Trans Aerosp Electron Syst*. 2003;39(4):1250–1262.
40. Lee KW, Ramasamy S, Singh SN. Adaptive sliding mode 3–D trajectory control of F/A–18 model via SDU decomposition. In: *Proceedings of the AIAA Guidance, Navigation, and Control Conference and Exhibit*. 2008; Honolulu, HI.
41. Miele A. *Flight Mechanics: Theory of Flight Paths*. Addison–Wesley; 1962.
42. Etkin B. *Dynamics of Atmospheric Flight*. Wiley; 1972.
43. Bhat SP, Bernstein DS. Geometric homogeneity with applications to finite–time stability. *Math Control Signals Syst*. 2005;17:101–127.
44. Defoort M, Floquet T, Kokosy A, et al. A novel higher order sliding mode control scheme. *Syst Control Lett*. 2009;58:102–108.

Citation: Lee KW, Raj K, Singh SN. Robust nonlinear spatial trajectory control of F/A-18 model. *Aeron Aero Open Access J*. 2026;10(3):145–153.
DOI: 10.15406/aaoaj.2026.10.00262